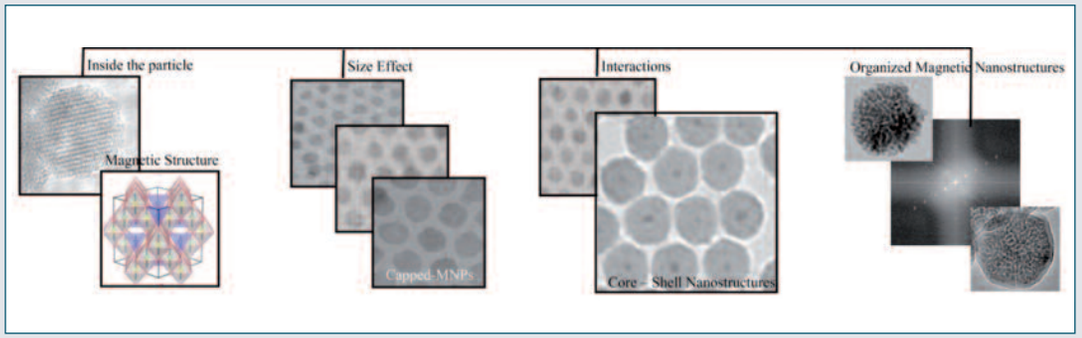

Carla Cannas, Davide Peddis
Dipartimento di Scienze Chimiche e Geologiche
Università di Cagliari
ccannas@unica.it
dpeddis@hotmail.com

DESIGN OF MAGNETIC SPINEL OXIDE NANOARCHITECTURES

Understanding the interplay among chemical, microstructural and physical properties is the key to design new materials. In this framework the intrinsic versatility of chemical science can give a wide and at the same time deep view, allowing to correlate synthesis and properties. This contribution focuses on the design of magnetic nanostructured spinel oxides, describing how to manipulate the matter to realize nanoarchitectures, in order to govern the magnetic properties.

Magnetic materials have been fascinating human beings for over 4,000 years. Since an ancient Greek shepherd noticed in Magnesia that the iron nails in his shoe and the iron tip of his staff stuck to certain rocks (Ladestone) [1], the magnetic phenomena have been object of increasing interest and the magnetic materials have found their way into almost every part of our civilization. In the last 40 years the development of new materials at smaller and smaller length scale has been at the root of progress in material science. In fact, a physical property depends on the size of an object, if its size is comparable to a dimension which is relevant to that property. In magnetism, typical sizes are in the nanometer range, leading to a drastic change of magnetic properties at the nanoscale [2]. In this context, nanostructured magnetic materials are one of the most vital and fastest growing research field and have great potential in biomedicine [3], magnetic data storage [4, 5], catalysis, magnetic sensoristic, ink industry, magneto-optics and spintronic [6].

Design of magnetic nanostructures for specific applications means to control the matter at the nanoscale, correlating microstructure and magnetic properties. In this view, this review describes some general concepts about magnetism and synthesis of inorganic nanoparticles. Then, in order to highlight the main factors influencing magnetic properties of spinel oxides nanoparticles (magnetic structure, chemical composition, particle size, interparticle interactions), structural and magnetic features of selected systems will be discussed. Finally, using nanoparticles as building blocks, an example of 3D magnetic superlattice, which represents the challenge for making a new generation of materials, will be given.

How to design magnetic nanoarchitectures

Magnetic properties of nanostructured spinel oxide: an overview

Minimization of energy provides a basis for predicting the direction of events in the universe. This is why a ferromagnet, in order to minimize its energy, is organized in a certain number of small regions, with different size and shape, called domains (i.e. uniformly magnetized regions having atomic magnetic moment oriented in the same direction). Magnetic domains have random directions so that the sum of overall domain moments is essentially zero [7]. Two adjacent domains are separated by a transition regions, called domain walls, in which the spins gradually rotate, from one domain to the other. By reducing particle size below a critical radius, when the dimension of the crystal is of the same order as that of the domain wall, a magnetic monodomain organization is energetically more favourable.

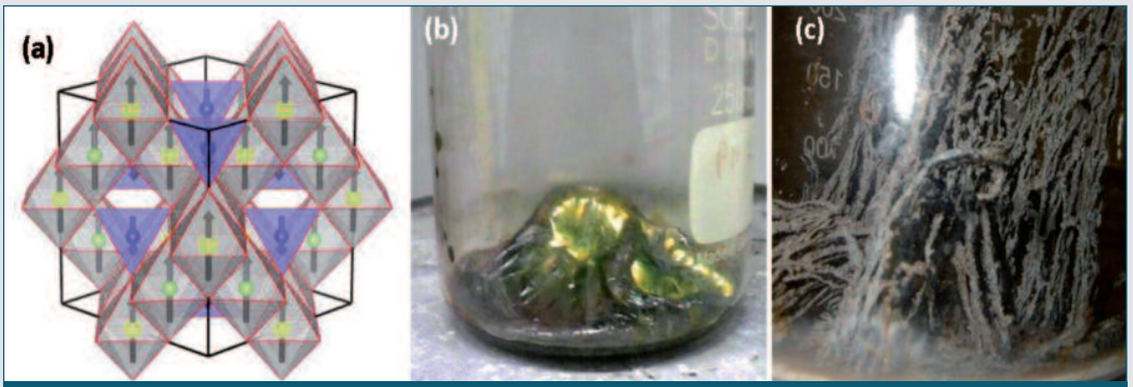

Fig. 1 - Schematic representation of spinel structure highlighting octahedral (gray) and tetrahedral (blue) interstitial sites (a); sol-gel auto-combustion route: evolution of the self-combustion reaction through a flameless process (b) and final voluminous and branched product (c)

A magnetic mono-domain particle (i.e. particle that is in a state of uniform magnetization at any field) can be considered as "*superspin*" with a magnetic moment, depending on the particle volume, expected in the range 10^3-10^5 Bohr magneton (μB). The magnetic behavior of an assembly of superspins depends on the type (e.g. dipolar interaction, exchange interaction) and the strength of the interactions among the magnetic entities [8]. On the other hand, in a system consisting of non-interacting mono-domain particles, the magnetic "*supermoment*" associated at each particle acts independently. They are characterized by the instability of magnetization due to thermal agitation, that for isolated spherical particle results in the flip of magnetization between its antiparellel easy directions, separated by an energy barrier (ΔE_a). This phenomenon is analogous to paramagnetism but, involving superpins, it is characterized by different time and magnetization scale, and for this reason it is called *superparamagnetism*. The rate of the magnetization flipping is governed by the Néel expression [9]:

$$\tau = \tau_0 \exp(\Delta E_a / k_B T) \quad (1)$$

where k_B is the Boltzmann constant and τ_0 is a constant depending on the intrinsic features of the material. An assembly of mono-domain particles shows superparamagnetic behavior above a certain temperature ($k_B T >> \Delta E_a$), labeled blocking temperature, T_B, while below this temperature ($k_B T << \Delta E_a$) magnetic properties are similar to those of the bulk material. The heart of the equation (1) is the energy barrier ΔE_a that, for an isolated particle, can be considered directly proportional to particle volume (V) and to magnetic anisotropy of the material (K). The term magnetic anisotropy describes the dependence of the internal energy on the direction of the magnetization, leading to the formation of *easy* (minimum of energy) and *hard* (maximum of energy) axis. For bulk materials magnetic anisotropy energy depends mainly on structure and chemical composition (i.e. magnetocrystalline anisotropy); for magnetic nanoparticles other factors, as particles shape (i.e. shape anisotropy) and high surface on volume ratio (i.e. surface anisotropy) should be also considered. In summary, magnetic properties of non-interacting nanoparticles can be governed by the control of the energy barrier and therefore by tuning V (particle size, particle size distribution) and K (magnetic structure, chemical composition, shape of the particles and surface effects).

Among the relevant features of the size reduction of magnetic particles, the presence of magnetic disorder deserves a special attention, as it determines strong modifications in the magnetic properties.

In seventies J.M.D. Coey wrote that "*ultrafine particles may be visualized as having a core with the normal spin arrangement, and a surface layer in which the spin of the ions are not oriented at random, but are inclined at some angle to their normal direction*" even if "*some canting in the interior cannot be excluded*" [10]. Since that time, the presence of non-collinear spin structure (*spin-canting*) in nanoparticles has been intensively studied and the landscape sketched out by Coey has been completed and detailed [11, 12].

Among magnetic iron oxides, the compounds with spinel structure ($Me^{(II)}Fe_2^{(III)}O_4$; $Me^{(II)}$ = Co^{2+}, Ni^{2+}, Fe^{2+}, Zn^{2+}, etc.) represent probably the most important class, because the rich crystal chemistry of spinels offers excellent opportunities for fine tuning the magnetic properties. Spinels have a face-centered cubic (fcc) structure, in which the oxygen atoms are cubic close-packed. The structure contains two interstitial sites, occupied by metal cations, with tetrahedral, *(T)*-site, and octahedral, *[O]*-site, oxygen coordination, resulting in a different local symmetry [13] (Fig. 1a). The magnetic properties of oxides with spinel structure can be understood and controlled through magnetic coupling. In fact, super-exchange interactions between atomic magnetic moments in T (J_{TT}) and O (J_{OO}) interstices lead to a ferromagnetic ordering between the ions located in the two sites, respectively, giving rise to two magnetic sub-lattices (Fig. 1a). On the other hand, interactions between magnetic ions in the T and O sites (J_{TO}) induce antiferromagnetic order, and are tenfold higher than the J_{TT} and J_{OO} interactions. Then, the dominant intra-lattice J_{TO} interactions induce a non-compensated antiferromagnetic order (i.e. ferrimagnetism) between the T and O sub-lattices (Fig. 1a). Therefore, the net magnetization can be considered proportional to the difference between the T and O sub-lattice magnetizations. The coupling is, in turn, closely related to the cationic distribution and to the chemical composition of the materials. Even small changes in the cationic distribution in compounds with the same chemical composition, can result in substantial changes of magnetic properties [14]. The magnetic anisotropy is also related to the cationic distribution because the single-ion anisotropy depends on its interstitial site [15, 16]. Moreover, by adjusting the chemical identi-

ty of $Me^{(II)}$, the magnetic configuration of $Me^{(II)}Fe_2O_4$ can be chemically engineered, obtaining a wide range of magnetic behaviors. Thus, we can define the magnetic structure in spinel nanoscaled systems as due to the complex interplay between cationic distribution and spin-canting.

How to fabricate spinel oxide nanoparticles

To manipulate the matter at the nanoscale, in the last twenty years a great number of synthetic strategies have been developed and optimized [17-21]. Among the several chemical strategies, sol-gel [22-24], micellar [25, 26], surfactant assisted high temperature decomposition techniques [27] and their suitable combinations have been proposed to design a great variety of spinel oxide based nanostructured materials [23, 28].

Sol-gel self-combustion (*SC*) route [29, 30] is very attractive for its versatility and has been used in several variations for the synthesis of pure and mixed oxide nanostructured materials [29-31]. This procedure has the advantages of inexpensive precursors, simplicity, short preparation time and moderate heating; furthermore large quantities of products can be easily prepared. It involves the use of metal nitrates, a ligand like citric acid and ammonia. The gels resulting from the cross-linking of metal-carboxylate complexes, when submitted to the appropriate heating, go through a self-propagating flameless combustion reaction (Fig. 1b) which converts the gel into a branched voluminous product (Fig. 1c). Changing the composition of the starting mixture, pH of the sol and starting combustion temperature can produce final materials with different physical properties. The main limit of this synthetic approach is related to the low degree of control to the particles nucleation and growth phases, then obtaining large particle size distribution. This drawback can be partially overcome embedding magnetic phase in a crystalline or amorphous matrix by a proper combination of the sol-gel self-combustion technique with a conventional alkoxide sol-gel process [22]. The alkoxide, as matrix precursor, reacts with water in which metal nitrates, citric acid and ammonia are dissolved, and due to the sequence of hydrolysis and condensation reactions and to the polymerization of the carboxylate-metal complex, an homogeneous gel can be formed. Then, thermal treatments at moderate temperature (250-300 °C), induces a self-propagating combustion process which leads to final product in a very short time. The method has been extensively used in the synthesis of Fe_2O_3 and $CoFe_2O_4$ silica composites with very high surface area [30, 32]. The *nanocompositing* process not only allows a reduction in particles aggregation but also provides a way to control the structure, the morphology and consequently the magnetic properties of the material. Therefore, particle size and particle size distribution can be tuned, within certain limits, both by changing the concentration of magnetic phase and/or by suitable thermal treatments [30].

The control of micro-structural features at the nanoscale can be better governed by surfactant assisted solution phase methods, allowing to obtain nanoparticles with controlled structure, composition particle size and shape [27, 33-37].

Micellar methods have been used to prepare a wide range of spinel ferrite nanoparticles with narrow size distribution [25, 26, 36]. Both direct (*DM*) and reverse micelles (*RM*) involve the use of surfactants with a concentration above the critical micelle concentration (CMC). Metal oxide nanoparticles are synthesized by reactions favored by the exchange dynamics of solute (metal salt and a precipitation agent) among micelles and/or with the continuous phase. The presence of the surfactant and the use of low temperatures (25-80 °C) allow to better control the nucleation kinetics as well as the growth phase; therefore small metal oxide particles of different shapes with narrow particle size distribution can be obtained. The normal micelle method can result appropriate also for the achievement of spherical nanostructures. In fact, the surfactant is recognized to play a fundamental role, inducing the assembling of the primary nanoparticles in secondary organized assemblies, with iso-oriented and porous structure [36, 37]. Furthermore, by the proper combination of the alkoxide sol-gel method and inverse micellar route, it is possible to coat homogeneously the metal oxide phase with amorphous silica (core-shell nanostructures) [37]. In spite of the high number of advantages shown by micellar approaches, due to the low synthesis temperature, often a low degree of crystallinity is observed.

Since 2002 [38] a further advance in the control of microstructural features and crystallinity of nanoparticles has been given by a synthetic strategy based on the high temperature decomposition (*HTD*) of metallorganic precursors (acetylacetonates) in the presence of surfactants (oleyalammine, oleic acid) in an organic high boiling temperature solvent (octadecene, benzyleter, phenyl ether).

The reason of the formation of nanocrystals with a narrow particle size distribution is due to the possibility to separate the nucleation step from the growth on existing nuclei. The temperatures has to be kept high enough to decompose the metal precursors (~200 °C), transforming them into atomic or molecular entities (monomers) with concentration above the nucleation threshold. For crystalline nanoparticles to form, the temperature for growth of the nanocrystals must be chosen to be high enough (280-320 °C) to promote the atomic rearrangement and annealing. The size of the nanoparticles is therefore strictly related to the metal precursors and to the thermal steps. Sizes can be further tuned by a seed-mediated growth process to obtain larger particles.

Magnetic structure and chemical engineering: inside the nanoparticle

Cationic distribution and magnetic disorder

With aim to exploit the magnetic behavior at the nanoscale several studies on $CoFe_2O_4/SiO_2$ nanocomposites prepared by sol-gel self-combustion route set up in our laboratories have been carried out [15, 30, 32, 39]. Specifically, in order to highlight the influence of magnetic structure on magnetic properties, two nanocomposites treated at 900

°C with 10 and 5 weight percent of $CoFe_2O_4$ (*$F10_{SC}$*, *$F5_{SC}$*) have been selected. TEM and HRTEM analysis on both samples shows crystalline nanoparticles homogeneously dispersed in silica matrix (Fig. 2a), with log-normal distributed diameters and similar mean particle size (<*DTEM*> ~3 nm) (Tab. 1). Magnetic characterization confirms this picture, showing substantially equal blocking temperature, T_B, (Tab. 1) and absence of interparticle interactions [39, 40]. These features allow to study the magnetic structure of the nanoparticles, regardless of the influence of particle size and interparticle interactions. The investigation of the magnetic structure can be carried out by using ^{57}Fe Mössbauer spectroscopy, based on the nuclear Zeeman splitting caused by the internal magnetic field at the site of the iron nucleus. In particular Mössbauer spectra of ferrites in intense applied fields allow to distinguish *T*- and *O*-site components.

As an example, Fig. 2b shows ^{57}Fe Mössbauer spectra recorded without field (black symbols and line) and under a magnetic field (red symbols and line) parallel to the γ-ray directions for *$F10_{SC}$* sample: lines 1 and 6 are split in the in field-spectrum, allowing to distinguish the iron atoms located in *T* and *O* sites and then to determine the cationic distribution. In-field spectrum provides information also on spin-canting. In fact, in the presence of an external magnetic field parallel to the γ-ray direction, the relative areas of the six lines give information about the degree of alignment of the atomic spins with the applied field. When the lines 2 and 5 have non-zero intensity, a non-collinear spin structure is suggested, and the fraction of canted spins and the mean canting angle with respect to external field can be evaluated [15, 39]. In Tab. 2 the most important parameters obtained by the fitting of Mössbauer spectra recorded at 6 K under a magnetic field (6 T) for both samples are reported. Spectra were fitted assuming perfect ferrimagnetic local environments for some of the iron atoms; thus, the relative area of lines 2 and 5 was constrained to zero for two sextets corresponding to *T* (sextet 1) and *O* sites (sextet 2). A third sextet (sextet 3) was introduced to represent the iron ions with canted spins [15, 39, 41]. Despite the same mean particle size, the two samples have quite different cationic distribution. In addition, the *$F5_{SC}$* shows an higher fraction of canted spins and higher mean canting angle (Tab. 2). This can be ascribed to the fact that the self-combustion reaction occurs in slightly different ways in the two samples. Thermal analysis of the precursors indicates a different speed of the particle formation and growth of the particle that might induce differences in cationic distribution and spin-canting. In fact, ultra-small particles are very sensitive to these effects, and even small differences in the thermal history of the material can induce relevant modifications in the cationic distribution [30]. The values of effective magnetic field and isomer shift (Tab. 2) extracted from in-field Mössbauer spectra are equal, within the experimental error, for sextet 2 and sextet 3, suggesting that the canted spins are mainly located in the *O* sites. These results lead to a complete description of the magnetic structure of the nanoparticles. As an example the magnetic structure at of the *$F10_{SC}$* samples at 5 K is sketched in Fig. 2c where 17% of the iron spins located in *O* sites are frozen with a mean angle of 37° with respect to the external field. The knowledge of the magnetic structure of the nanoparticles allows to describe the macroscopic properties of the material, as for example saturation magnetization. Despite of same mean particle size, *$F5_{SC}$* and *$F10_{SC}$* samples have different values of M_s at 5K (*$F5_{SC}$* ≈ 109 Am^2kg^{-1}; *$F10_{SC}$* ≈ 94 Am^2kg^{-1}), with the most diluted nanocomposite showing value higher than bulk value (~90 Am^2kg^{-1}). Starting from cationic distribution, assuming that Fe^{3+} and Co^{2+} have a magnetic

Tab. 1 - Mean Particle Size from TEM data (⟨D_{TEM}⟩); blocking temperature from (T_B); experimental (exp.) and calculated (th.) magnetic moment × formula unit $\mu_{C,F}$

Sample	<D_{TEM}> (nm)	T_B (K)	$\mu_{C.F.}$ exp (μ_B)	$\mu_{C.F.}$ th (μ_B)
$F5_{SC}$	2.8 (3)	17 (1)	5.6	5.4
$F10_{SC}$	2.9 (3)	18 (1)	4.7	5.0

Uncertainties in the last digit are given in parentheses

Tab. 2 - Effective magnetic field (B_{eff}); isomer shift (δ); relative area of the lines 2 and 5 for each component ($A_{2,5tot}$); mean canting angle (<θ>) and cationic distribution (uncertainties in the last digit are given in parentheses)

Sample	Spectral Comp.	B_{eff} (T)	δ (mm/s)	$A_{2,5Tot}$ (%)	<θ> (°)	Cationic Distribution
$F5_{SC}$	Sextet 1 x (T site)	57.8(2)	0.39(3)	32(1)	42(1)	$(Co_{0.80}Fe_{0.20})[Co_{0.20}Fe_{1.80}]O_4$
	Sextet 2 x (O site)	49.4(1)	0.46(2)			
	Sextet 3 (Canted Spin)	49.5(3)	0.46(5)			
$F10_{SC}$	Sextet 1 x (T site)	55.7(3)	0.37(4)	17(1)	37(1)	$(Co_{0.56}Fe_{0.44})[Co_{0.44}Fe_{1.56}]O_4$
	Sextet 2 x (O site)	47.0(2)	0.48(3)			
	Sextet 3 (Canted Spin)	48.3(5)	0.53(7)			

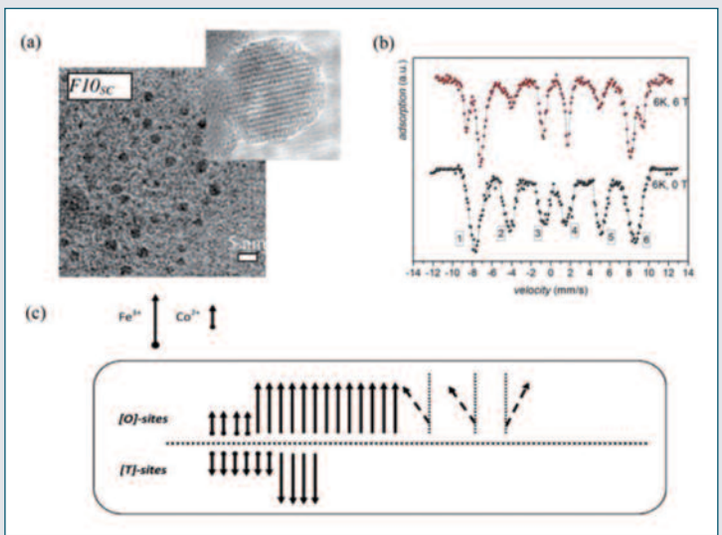

Fig. 2 : *TEM* and *HRTEM* images of *$F10_{SC}$* sample (a); Mössbauer spectra recorded at 6 K without field (black) and under an applied field of 6T (red) parallel to the γ-ray direction (b) schematic representation of magnetic structure of $F10_{SC}$ sample as obtained by Mössbauer measurements in high field (c)

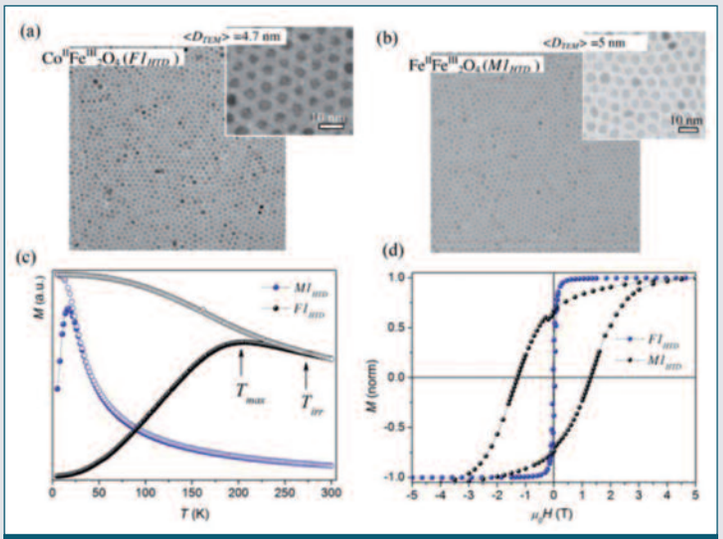

Fig. 3 - Bright field *TEM* images of $CoFe_2O_4$ nanoparticles ($F1_{HTD}$) (a); Bright field TEM images of Fe_3O_4 nanoparticles ($M1_{HTD}$) (b); *ZFC* (full symbols) and *FC* (empty symbols) magnetizations for $F1_{HTD}$ (black) and $M1_{HTD}$ (blue) recorded with an applied field of 2.5 mT (c); Hysteresis loops at 5K for $F1_{HTD}$ (black) and $M1_{HTD}$ (blue).

moment of 5 μB and 3 μB [42] respectively, and considering that each canted spin will give a mean contribution to saturation magnetization depending on the canting angle θ (M_{eff}=M_{atomic} x *cos*θ), value of M_s can be calculated. In Tab. 1, theoretical (*th.*) and experimental (*exp.*) M_s values, expressed in magnetic moment x chemical formula (μ*c.f.*), are reported, showing a very good agreement.

Saturation magnetization is one of the most important magnetic features for application of nanoparticles in biomedicine and catalysis [3, 14]. The strong expected reduction of M_s observed at the nanoscale [40, 43] in our sample has been overcome, obtaining value similar to the bulk materials, by the presence of localized canting in *O*-sites and by the control of cationic distribution.

Chemical engineering

In order to study the effect of chemical composition on magnetic properties, magnetite ($M3_{HTD}$) and cobalt ferrite ($F3_{HTD}$) nanoparticles with similar particle diameter, prepared by *HTD* method, have been selected [37]. TEM analysis indicates the formation of spherical and uniform nanoparticles self-assembled in hexagonal close-packed superlattice, due to the high degree of uniformity in diameter (Fig. 3 a-b). Particle size has normal distribution of diameters with similar mean particle size (Tab. 3). An overview on magnetic behavior of nanoparticles can be obtained by measurements of magnetization versus temperature, performed by zero field-cooled (ZFC) and field-cooled (FC) protocols.

The ZFC protocol consists of cooling the sample in a zero magnetic field from high temperature (where all the particles are in superparamagnetic state) to the lowest measuring temperature. Then, a static magnetic field is applied and magnetization is measured during the warming up. The resulting curve is termed ZFC (Fig. 3c full symbols) because the sample has been previously cooled in the absence of a magnetic field. When the sample is cooled below the blocking temperature without an applied magnetic field, all the atomic magnetic moments in each single-domain particle point along the nanoparticle easy axis. Magnetic anisotropy acts as an energy barrier to prevent the switching of magnetization from the easy axis. Due to the high number of particles and the random distribution of the easy axis directions, the average magnetization is almost zero [14]. When the temperature increases, the magnetic anisotropy in some nanoparticles is overcome and the magnetization directions of these thermally activated nanoparticles start to align with the applied field. As a consequence, the total magnetization initially increases with increasing temperature. The ZFC curve then exhibits a maximum, and the corresponding temperature (T_{max}) is, for non-interacting particles, directly proportional to the average blocking temperature ($T_{max} \propto T_B$) [44].

Conversely, the FC protocol consists of cooling the sample in a small static field and measuring the magnetization during warming up, without removing the field. When a magnetic field is applied during the cooling process, all the net magnetic moments of the nanoparticles are aligned along the field direction, regardless of the easy axis directions of each individual nanoparticle. As the nanoparticles are cooled at low temperature, the magnetization direction of each particle is frozen in the field direction. By increasing the temperature, an increasing number of particles will be in superparamagnetic state and the magnetization will decrease monotonically (M_{FC} in Fig. 3c, empty symbols). Below a certain temperature, the ZFC and FC curves diverge and an irreversible magnetic behavior is observed. This temperature, called *irreversibility temperature* (T_{irr}), can be related to the blocking temperature of the biggest particles. T_{irr} can be also considered as the onset temperature above which all nanoparticles start to behave as superparamagnets.

Despite similar mean particle size, temperature dependences of magnetization measured by ZFC and FC protocol have completely different features. In particular, the temperature corresponding to the maximum in ZFC curve has a strong increase in cobalt ferrite sample (Tab. 3), indicating an incresing of $\Delta E_a \propto KV$. For spherical particles with similar size, ΔE_a increasing can be only ascribed to a strong increse of anisotropy (K). This picture is confirmed by field dependence of magnetization at 5 K (Fig. 2d), showing an hysteretic behavior with coercive field value (i.e. the magnetic field to which corresponds a magnetization equal to 0) in $F3_{HTD}$ about 60 times higher with respect $M3_{HTD}$. The high coercivity observed in the $CoFe_2O_4$ sample can be associated to the strong magnetocrystalline contribution of Co^{2+} ions ($3d^7$), which have a non-zero orbital momentum [45].

Generally speaking, the control of the magnetic anisotropy represents

Tab. 3 - Mean particle size from TEM data ($\langle D_{TEM} \rangle$); Temperature corresponding to the maximum in ZFC curve (T_{max}); coercive field (H_c) recorded at 5 K

Sample	$\langle D_{TEM} \rangle$ (nm)	T_{MAX} (K)	$\mu_0 H_c$ (5K) (T)
$F3_{HTD}$	4.4 (1)	207 (5)	1.29 (3)
$M3_{HTD}$	4.3 (1)	17 (4)	30 mT (2)

Uncertainties in the last digit are given in parentheses

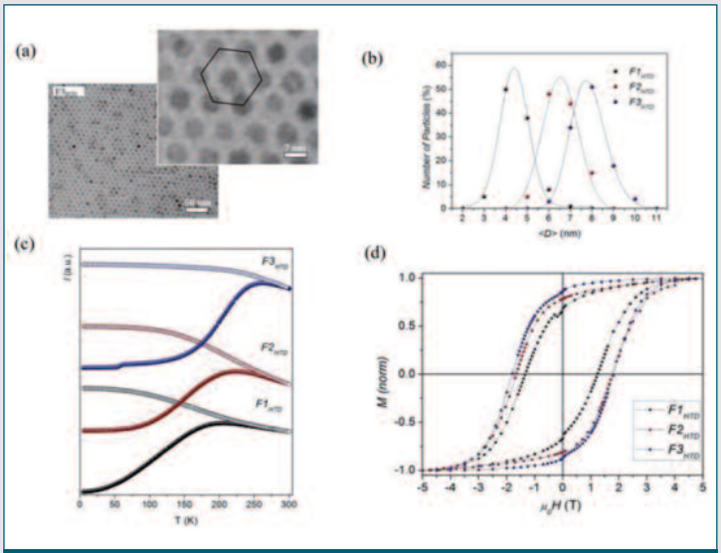

Fig. 4 - Bright field TEM images of $CoFe_2O_4$ nanoparticles ($F3_{HTD}$) (a); Particle size distribution extracted from TEM images (b); ZFC (full symbols) and FC (empty symbols) magnetizations for $F1_{HTD}$ (black) $F2_{HTD}$ (red) and $F3_{HTD}$ (blue) recorded with an applied field of 2.5 mT (c); Hysteresis loops at 5K of $F1_{HTD}$ (black) $F2_{HTD}$ (red) and $F3_{HTD}$ (blue).

an important goal for application of magnetic nanoparticles in several fields, as magneto recording. In fact, to have small particles with T_B higher than room temperature (i.e. working temperature of magnetic memories) allows "*to beat the superparamagnetic limit*" [46], that is one of the main drawback to overcome, for the development of new nanostructured material in this field.

Particle size: evolution of the magnetic properties

Among the several synthetic approaches proposed in the literature, surfactant-assisted high temperature decomposition of metallorganic precursors allows to have a careful control of particle size and particle size distribution. A set of three $CoFe_2O_4$ samples ($F1_{HTD}$, $F2_{HTD}$, $F3_{HTD}$) with increasing particle size has been prepared by this method. The X-ray diffraction data indicates the presence of a unique $CoFe_2O_4$ phase with a cubic spinel structure (PDF Card 22-1086) [37] and an average crystallite size of 5.0, 6.0, 7.6 nm (Tab. 3, Fig. 4a). Particle size distributions obtained by bright field mode TEM micrographs show a normal distributed particles diameter (Fig. 4b), with evaluated mean value of 4.6, 6.5 and 7.8 nm for $F1_{HTD}$, $F2_{HTD}$ and $F3_{HTD}$ samples respectively (Tab. 4). The good agreement between $\langle D_{XRD}\rangle$ and $\langle D_{TEM}\rangle$ indicates the high degree of crystallinity of the particles. A decrease of polydispersity is observed increasing particle size (Tab. 4) and this can be directly correlated with the synthesis parameters. In fact, in order to obtain different particle size, starting mixtures have been firstly heated at 200 °C for 30 min ($F1_{HTD}$), 1h ($F2_{HTD}$) and 2h ($F3_{HTD}$). This trend confirms the suggestions reported in literature that indicate as better mono-dispersion can be obtained increasing the time length of the first thermal step at 200 °C [27]. With the increase of particle size, T_{max} (Tab. 4) increases and this can be mainly ascribed to increase of particles volume (equation 1), even if the influence of interparticle interactions should be taken into account. As expected, irreversible temperatures follow the same trend of T_{max} (Fig. 4c), indicating superparamagnetic behaviour at room temperature for all the samples. Field dependence of magnetization investigated a 300 K shows completely reversible behavior, (i.e. zero remanence magnetization and zero coercivity) confirming that all the sample are in superparamagnetic state. Conversely at 5 K, being the nanoparticles in the blocked state, all the samples show an hysteretic behavior (Fig. 4d). Saturation magnetization (M_s) and coercive field (H_c) are reported in Tab. 4. M_s values are lower than the bulk one (~90 Am^2kg^{-1}) and they are almost independent from particles size in the investigated range [47]. Coercivity values, from 1.29 T to 1.81 T, increase as the particle size increases, showing an unexpected behavior. In fact, entering the nanoscale, the surface component (K_s) plays the key role in regulating the magnetic anisotropy, and usually H_c increases with the decrease of particle size. However, it is well known that the interactions between molecules and surface atoms of nanoparticles can induce modification on surface anisotropy, leading to a decrease of K_s [48]. In our sample the presence of the surfactant bound to the particle [37] reduces surface anisotropy; then the key role is played by the magnetocristalline component, leading to the observed increase of coercivity with particle size.

Interparticle interactions

The magnetic behavior of an assembly of nanoparticles is strongly affected by interparticle interactions and $CoFe_2O_4$ prepared by *HTD* method represents an ideal system also in order to show the effect of dipolar interactions on magnetic behavior of nanoparticles based system. In fact, the presence of surfactant at the nanoparticle surface keeps them isolated from each other by a coating layer of about 2 nm. Then, it is reasonable to suppose that in this system only dipole-dipole interactions are present, as experimentally confirmed by remanent magnetization measurements [37, 49].

In a sample of randomly distributed nanoparticles with average magnetic moment μ and average separation d, the energy due to dipole-dipole interaction for one particle is on the order of [50, 51]:

$$E_{dip} \approx (\mu_0/4\pi)(\mu^2/d^3) \qquad (2)$$

Tab. 4 - Mean crystallite size from XRD data ($\langle D_{XRD}\rangle$); Mean particle size from TEM data ($\langle D_{TEM}\rangle$) and relative polidispersity (σ); temperature corresponding to the maximum in ZFC curve (T_{max}); irreversibility temperature (T_{irr}); coercive field (H_c) recorded at 5K; interaction dipolar energy (E_{dip})

Sample	$\langle D_{XRD}\rangle$ (nm)	$\langle D_{TEM}\rangle$ (nm)	σ (%)	T_{MAX} (K)	T_{IRR} (K)	$\mu_0 H_c$ (T)	E_{DIP} (K)
$F1_{HTD}$	5.0 (2)	4.4 (1)	17 (1)	207 (5)	247 (5)	1.29 (3)	8
$F2_{HTD}$	6.0 (3)	6.5 (1)	13 (1)	224 (4)	285 (4)	1.71 (2)	37
$F3_{HTD}$	7.6 (3)	7.8 (2)	10 (1)	262 (5)	283 (2)	1.81	60
$F3CS_{HTD}$	7.6 (3)	7.8 (2)	--	235 (5)	254 (4)	1.92	4

Uncertainties in the last digit are given in parentheses

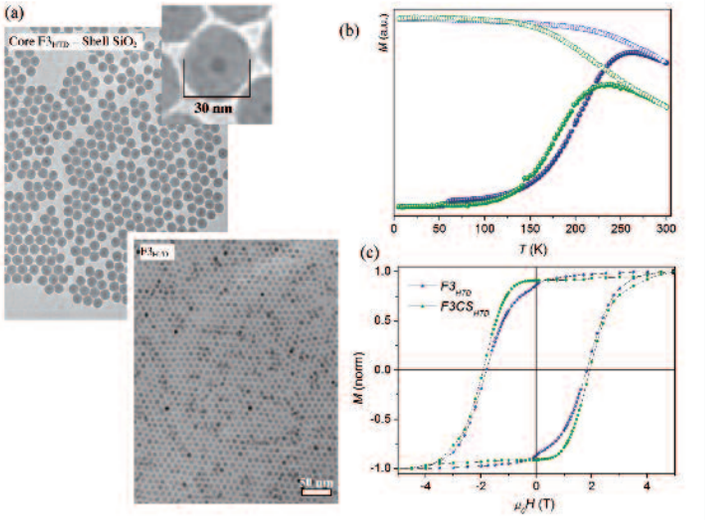

Fig. 5 - Bright field *TEM* images of a $CoFe_2O_4$ nanoparticles ($F3_{HTD}$) and $CoFe_2O_4/SiO_2$ core-shell nanoparticles ($F3_{HTD}CS$) (a); *ZFC* (full symbols) and *FC* (empty symbols) magnetizations for $F3_{HTD}$ (blue) and $F3_{HTD}CS$ (green) recorded with an applied field of 2.5 mT (c); Hysteresis loops at 5K for for $F3_{HTD}$ (blue) and $F3_{HTD}CS$ (green).

where μ_0 is the permeability of free space. Assuming a point dipole model (i.e. center to center maximum distance), a mean value of dipolar energy E_d/k_B (Tab. 4) has been calculated using equation (2) and defining the magnetic moment of a mono-domain particle as $\mu = M_S \times V$. An increase of dipolar energy is observed going from $F1_{HTD}$ to $F3_{HTD}$ samples. This effect can be ascribed mainly to a volume effect (increase of μ), because the interparticle separation is equal in all the samples due to the molecular coating. This is reflected by the *FC* curves (Fig. 4c) that show a temperature independent behavior below certain temperature, that increases with the increase of the interparticle interactions. In addition, it is important to underline that for all the samples, E_{dip}/k_B is well lower than T_{max}, indicating that superparamagnetic relaxation is mainly governed by magnetic anisotropy energy of the nanoparticles.

In order to isolate the effect of interparticle distance on interparticle interactions, silica coating of the $F3_{HTD}$ sample has been achieved by a suitable combination of sol-gel and microemulsion methods ($F3_{HTD}CS$) [35, 37]. TEM images in bright field mode (Fig. 5a) show the formation of spherical core/shell structures with an average overall size of 30 nm and a polidispersity of 5% with a single magnetic core in the center of the spheres. TEM images in dark field mode confirms the high degree of crystallinity of the core and the amorphous nature of the shell, that was also observed by XRD. The assembling of the nanoparticles appears to be in the form of hexagonal close packing. Silica coating [37] does not induce any changes on morpho-structural features of the particle, having as main effect to increase the interparticle distance. This reduces the strength of interparticle interactions, as confirmed by the strong decrease of dipolar energy calculated on the $F3CS_{HTD}$ sample (Tab. 4). The control of interparticle interactions represents an useful tool in order to tune the magnetic properties of the materials. Reducing of interactions leads to a decrease of blocking temperature, as indicated by the decrease of T_{max} in ZFC curves (Fig. 5b). In addition, the decrease of interactions influences also the reversal of magnetization leading to an increase of coercivity (Fig. 5c) [31, 52]. Fundamental studies on interparticle interactions, have a strong interest from a technological point of view. In fact, for several applications, concentrated assemblies of individually responding magnetic entities are required. This last requirement is difficult to be satisfied as interparticle dipole-dipole interactions are strongly enhanced mainly due to an increase in their concentration.

Organized magnetic nanostructures

The size and tunable properties of magnetic nanocrystals make them ideal building blocks for ordered nanostructured superlattices (*SPls*), which represent a great opportunity for making a new generation of tailored materials with completely new physical properties [53, 54]. In this complex framework, the major role in the collective physical behavior of *SPls* is played by magnetic interactions among nanoparticles. The realization of organized assemblies of nanoparticles with advanced functions requires the development of new and efficient approaches toward combining the ultra-small building blocks into desired structures.

The microemulsion surfactant assisted method has been used for the synthesis of $CoFe_2O_4$ samples, since it opens the way of regulating the size of the primary nanoparticles through the control of the reaction parameters and offers the possibility to assemble them using the influ-

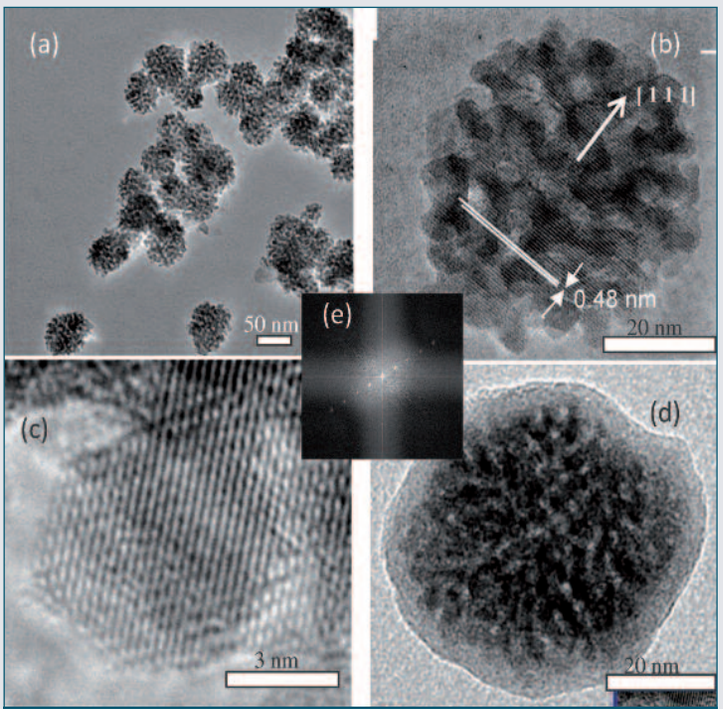

Fig. 6 - TEM image at low magnification of $CoFe_2O_4$ spherical nanoporous nanostructures (a), EFTEM image of an iso-oriented spherical assembly (b) EFTEM of a single primary cubic nanoparticle (c) TEM image of a single aggregate silica coated nanostructure (d) FFT of the uncoated $CoFe_2O_4$ nanostructure (e)

ence of the surfactant [35, 36]. Suitable synthesis conditions lead to the formation of spherical aggregates of about 50-60 nm (*FMD* sample) in diameter (Fig. 6a) composed of cubic shaped nanocrystals (Fig. 6c). TEM images show crystallites with an average size of 7.3 nm (polydispersity of 14%) forming twin crystals with shared edges. The structure of the aggregates shows worm-like nanopores with pore size of about 2-3 nm (Fig. 6a-d) [4]. The high-resolution images show that parallel lattice fringes are uniformly extended over each aggregate, indicating that primary nanoparticles are organized into an iso-oriented structure (Fig. 6b). This is further confirmed by the FFT image showing symmetrically aligned spots (Fig. 6e) [4]. A sol-gel Igepal/cyclohexane/water microemulsion, has been used to coat aggregates with a silica layer (FCS_{MD}). TEM analysis indicates the efficiency of this procedure, showing spherical aggregates of nanoparticles, homogeneously covered by a 7-8 nm thick silica shell (Fig. 6d).

Through the combined investigation of time dependence of magnetization (relaxation measurement) and field dependence of remanent magnetization, it is possible to obtain information about the volume of the material involved in the process of overcoming the energy barrier for magnetization reversal (i.e. activation volume) [54].

The calculated value of the activation volume is 275 nm^3, corresponding to a cubic particle with an edge of 6.5 nm. This value is very close to that measured using HRTEM images, i.e. the magnetic volume actually coincides with the physical volume of the primary nanoparticles inside the aggregates. This result indicates that exchange interactions are absent despite the intimate contact among particles and the iso-oriented structure.

This would be associated with the high degree of porosity of the aggregates, as also evidenced by the high BET specific surface area (160 m^2/g). In conclusion these spherical porous aggregates of iso-oriented nanoparticles present advantages of 3D superlattice as high magnetic moments, and the improved magnetic properties of small particles as high anisotropy (H_C *(5 K)* = 0.66 T).

Final remarks

Exploring, understanding and exploiting the complex behavior in magnetic materials at nanoscale is the key and the challenge not only for fundamental research, but it is crucial for technological applications. For example, in biomedical applications, such as MRI contrast agents, magnetic nanoparticles should be superparamagnetic at room temperatures in order to avoid agglomeration. However, the superparamagnetic state must be avoided in high-density information storage since superparamagnetic relaxation cause the magnetic moment fluctuation and as a consequence the lost of the stored information.

Spinel ferrites are an ideal magnetic system to understand and govern magnetic properties through chemical manipulations, due to the strong sensitivity of their properties to the cationic distribution, spin-canting, interface, size changes, interactions. For this reason this contribution is aimed to elucidate, through a selected set of samples, the critical relationship between synthesis, microstructure and magnetic properties, and how, parameters like saturation magnetization, coercivity field, interactions can be tuned. This approach is essential as magnetic nanomaterials move into the next phase of innovative research with emphasis on development of new materials for future applications.

Acknowledgments: A special thank goes to Prof. Giorgio Piccaluga and Prof. Anna Musinu. D. Peddis is granted by RAS (Regione Sardegna - Centro Regionale di Programmazione) co-founded by PO Sardegna FSE 2007-2013 sulla L.R.7/2007 "Promozione della ricerca scientifica e dell'innovazione tecnologica in Sardegna".

Carla Cannas was born in Cagliari (Italy) in 1972. From 2002 she is Lecturer in General and Inorganic Chemistry (CHIM/03) at the Faculty of Science of the University of Cagliari. Her research activity has been main devoted to the design of inorganic magnetic and luminescent nanostructures through chemical synthesis (sol-gel, self combustion, micellar, surfactant assisted thermal decomposition routes and their suitable combination) and the study of structure-morphology-property relationships. She presented the results of her research in various national and international conferences, also as invited, and she is coauthor of about 60 scientific papers, a patent (Xerox Corporation) and a book chapter.

Davide Peddis was born in Cagliari (Italy) in 1976. He received the PhD in Physical-Chemistry in 2007 at the University of Cagliari. In the years 2007-2009 he was post-doctoral researcher at ISM - CNR (mentor Dr. D. Fiorani). He was visiting professor at the Le Mans University and Extended Guest Lecturer at the Uppsala University. Actually, he is Research Fellow at the University of Cagliari granted by Regione Autonoma della Sardegna. The scientific activity of D. Peddis focus on the physical chemistry of nanostructured magnetic materials and it is represented in 28 publications, one book chapter, and over 60 communications, also invited, to national and international conferences.

References

[1] Plinio il Vecchio, 23-79 d.C.
[2] D.L. Leslie-Pelecky, R.D. Rieke, *Chem. Mater.*, 1996, **8**, 1770.
[3] Q.A. Pankhurst *et al., J. Phys. D: Appl. Phys.*, 2003, **36**, R167.
[4] R.H. Kodama, *J. Magn. Magn. Mater.*, 1999, **200**, 359.
[5] J.I. Martín *et al., J. Magn. Magn. Mater.*, 2003, **256**, 449.
[6] G.C. Papaefthymiou, *Nano Today*, 2009, **4**, 438.
[7] S. Blundell, Magnetism In Condesed Matter, O.U. press, New York, 2003.
[8] S. Bedanta, W. Kleeman, *J. Phys. D: Appl. Phys.*, 2009, **42**, 013001.
[9] L. Néel, *Annales de Gèophysique*, 1949, **5**, 99.
[10] J.M.D. Coey, *Phys. Rev. Lett.*, 1971, **27**, 1140.
[11] A.H. Morrish, K. Haneda, *J. Magn. Magn. Mater.*, 1983, **35**, 105.
[12] E. Tronc *et al., J. Magn. Magn. Mater.*, 2000, **221**, 63.
[13] A.R. West Solid State Chemistry and its applications, Wiley, 1984.
[14] L. Suber, D. Peddis, Approaches to Synthesis and Characterization of Spherical and Anisometric Metal Oxide Magnetic Nanomaterials, in Magnetic Nanomaterials, Vol. 4, Wiley, Weinheim, 2010.
[15] C. Cannas *et al., J. Chem. Phys.*, 2006, **125**, 164714.
[16] J.C. Slonczewski, *J. Appl. Phys.*, 1961, **32**, S253.
[17] H.S. Nalwa Handbook of Nanostructured Materials and Nanotecnology, A. Press, San Diego, 2000.
[18] A.V. Goldstein Handbook of Nanophase Materials, M.D. Inc., New York, 1997.
[19] A.S. Edelstein, R.C. Cammarata Nanomaterials: Synthesis, Properties and Applications, I.P. Pubblishing, Bristol, 1996.
[20] B.L. Cushing *et al., Chemical Reviews*, 2004, **104**, 3893.
[21] P. Tartaj *et al., J. Phys. D: Appl. Phys.*, 2003, **36**, R182..
[22] C.J. Brinker, Sol-Gel Science, A. Press, New York, 1990.
[23] C. Cannas *et al., Phys. Chem. Chem. Phys.*, 2001, **3**, 832.
[24] C. Cannas *et al., J. Mater. Chem.*, 2002, **12**, 3141.
[25] C.R. Vestal, Z.J. Zhang, *International Journal of Nanotechnology*, 2004, **1**, 240.
[26] N. Moumen, M.P. Pileni, *Chem. Mater.*, 1996, **8**, 1128.
[27] S. Sun *et al., J. Am. Chem. Soc.*, 2004, **126**, 273.
[28] C. Cannas *et al., The Journal of Physical Chemistry B*, 1998, **102**, 7721.
[29] C. Cannas *et al., J. Nanop. Res.*, 2004, **6**, 223.
[30] C. Cannas *et al., Chem. Mater.*, 2006, **18**, 3835.
[31] C. Cannas *et al., J. Nanop. Res.*, 2006, **8**, 255.
[32] D. Peddis *et al., J. Phys. Chem. C*, 2008, **112**, 5141.
[33] T. Hyeon, *Chemical Communications*, 2003, 927.
[34] N. Feltin, M.P. Pileni, *Langmuir,* 1997, **13**, 3927.
[35] C. Cannas *et al., Chem. Mater.*, 2008, **20**, 6364.
[36] C. Cannas *et al., J. Colloid Interface Sci.*, 2010, **342**, 415.
[37] C. Cannas *et al., Chem. Mater.*, 2010, **22**, 3353.
[38] S. Sun, H. Zeng, *Journal of American Chemical Society*, 2002, **124**, 8204.
[39] D. Peddis *et al., J. Phys. Chem. B*, 2008, **112**, 8507.
[40] D. Peddis *et al., Nanotech.*, 2010, **21**, 125705.
[41] T.A. Anhøj *et al., J. Magn. Magn. Mater.*, 2003, **260**, 115.
[42] K. Haneda, A. H. Morrish, *J. Appl. Phys.*, 1988, **63**, 4258.
[43] A.E. Berkowitz *et al., J. Appl. Phys.*, 1968, **39**, 1261.
[44] J.I. Gittleman *et al., Phys. Rev. B*, 1974, **9**, 3891.
[45] N. Moumen *et al., J. Phys. Chem.*, 1996, **100**, 14410.
[46] V. Skumryev *et al., Nature*, 2003, **423**, 850.
[47] A.G. Roca *et al., Nanotech.*, 2006, **17**, 2783.
[48] F. Bødker *et al., Phys. Rev. Lett.*, 1994, **72**, 282.
[49] D. Peddis *et al., Chemistry - A European Journal*, 2009, **15**, 7822.
[50] S. Morup *et al., Beilstein Journal of Nanotechnology*, 2010, **1**, 182.
[51] M.F. Hansen, S. Mørup, *J. Magn. Magn. Mater.*, 1998, **184**, 262.
[52] R.D. Zysler *et al., J. Magn. Magn. Mater.*, 2000, **221**, 37.
[53] M.P. Pileni, *J. Phys. D: Appl. Phys.*, 2008, **41**, 134002.
[54] S. Laureti *et al., Nanotech.*, 2010, **21**, 315701.

RIASSUNTO

Design di nanoparticelle di ossidi con struttura spinello

La correlazione tra proprietà chimiche, fisiche e strutturali è alla base della comprensione delle leggi che governano la materia, ma è solo attraverso la manipolazione della materia stessa che questa comprensione si traduce in capacità di progettare nuovi materiali. In un quadro così articolato, l'intrinseca versatilità della chimica permette di mettere in relazione sintesi, struttura e proprietà, consentendo di progettare un materiale con caratteristiche specifiche.

Questo lavoro vuole rappresentare un contributo alla definizione delle linee guida per il design di nanoparticelle di ossidi con struttura spinello, descrivendo come il controllo delle dimensioni particellari, della struttura cristallina e la realizzazione di opportune nano-architetture consenta una modulazione delle proprietà magnetiche di questi materiali.